CHEMISTRY OF MATERIALS
Article

Chem. Mater. **2010,** *22,* 1831–1835 1831
DOI:10.1021/cm903355n

Vertically Aligned Single-Crystalline Ferromagnetic Ni_3Co Nanowires

Nitin Bagkar,[†] Kwanyong Seo,[†] Hana Yoon,[†] Juneho In,[†] Younghoon Jo,[‡] and Bongsoo Kim*,[†]

[†]*Department of Chemistry, KAIST, Daejeon 305-701, Korea, and* [‡]*Nano Materials Research Team, KBSI, Daejeon 305-333, Korea*

Received November 3, 2009. Revised Manuscript Received December 30, 2009

We report synthesis of vertical Ni_3Co nanowires on a *c*-plane sapphire substrate by chemical vapor transport method. A vapor−solid−solid mechanism was proposed for Ni_3Co nanowire growth, which was catalyzed by Ni_3Co_2 nanoparticle at the tip. As-synthesized vertically aligned single-crystalline Ni_3Co nanowires exhibit strongly ferromagnetic properties. Such single-crystalline ferromagnetic alloy nanowires could be important in the application of spintronics such as nonvolatile memory devices. We could also control the composition of the nanowire by adjusting experimental conditions, producing Ni, Ni_3Co, and NiCo nanowires.

Introduction

Nanowires (NWs) exhibiting ferromagnetism above room temperature are attractive candidates for magnetic storage, nanoelectronics, and spintronics applications.[1] Emerging spintronics technology utilizing magnetic moment to carry information has offered new types of devices superior to conventional electronic devices in performance.[2] Metallic spintronic devices such as hard disk read heads and magnetic random access memory represent information by magnetization direction in ferromagnetic metal nanostructures. The scope of spintronic devices can be further extended if the magnetic data bits in the form of domain walls (DWs) interact with each other and propagate along magnetic nanostructures. It is recently reported that ferromagnetic NWs aligned horizontally or vertically can offer significant advantage as a racetrack memory (RM) in which the pattern of magnetic domains acting as data bits is transported by applying highly spin polarized current.[3] The DW can move around when it interacts with spin-momentum torque generated by current passing through NWs. Such DW movement can be electronically controlled for possible application as a nonvolatile memory. The important parameters such as operational current density and DW dynamics in these devices are determined by the geometry and magnetic behavior of ferromagnetic NWs. It is critical to reduce the current density to move DWs because of adverse Joule heating effect, which is detrimental to device performance. The operational current density can be minimized by employing highly anisotropic metal NWs exhibiting single crystallinity,[4] sufficiently small (∼100 nm) diameter,[3] perpendicular magnetic anisotropy,[5] atomically smooth surface,[6] and an isotropic cross-section,[7] all of which will reduce greatly the domain pinning and energy barrier for DW movement. Hence alignment of ferromagnetic single-crystalline NWs in vertical directions and their optimum morphology control are highly desirable.

One-dimensional nickel cobalt alloy nanostructures have been synthesized by various template based methods.[8−11] Although some nickel cobalt nanostructures with shape anisotropy exhibit increased magnetic anisotropy,[12,13] most of these nanostructures did not satisfy the above criteria for integration into spintronics devices. The objective of present investigation was to synthesize single-crystalline, vertically aligned, and strongly ferromagnetic nickel cobalt NWs by chemical vapor transport method. Here, we present vapor−solid−solid (VSS) synthesis of vertical Ni_3Co NWs on *c*-plane sapphire substrates satisfying most of the above criteria for possible application as nonvolatile memory devices. To the best of our knowledge, this is the first report on the synthesis of twin-free, single-crystalline, and vertically aligned ferromagnetic NWs. Additionally, the composition of the NWs was tuned by changing the ratio of precursor amount for

*Corresponding author. E-mail: bongsoo@kaist.ac.kr.

(1) Prinz, G. A. *Science* **1998**, *282*, 1660.
(2) Wolf, S. A.; Awschalom, D. D.; Buhrman, R. A.; Daughton, J. M.; von Molnar, S.; Roukes, M. L.; Chtchelkanova, A. Y.; Treger, D. M. *Science* **2001**, *294*, 1488.
(3) Parkin, S. S. P.; Hayashi, M.; Thomas, L. *Science* **2008**, *320*, 190.
(4) Kim, K.-J.; Lee, J.-C.; Ann, S.-M.; Lee, K.-S.; Lee, C.-W.; Cho, Y. J.; Seo, S.; Shin, K.-H.; Choe, S.-B.; Lee, H.-W. *Nature* **2009**, *458*, 740.
(5) Jung, S.-W.; Kim, W.; Lee, T.-D.; Lee, K.-J.; Lee, H.-W. *Appl. Phys. Lett.* **2008**, *92*, 202508.
(6) Kim, K.-J.; Choe, S.-B. *J. Magn. Magn. Mater.* **2009**, *321*, 2197.
(7) Tatara, G.; Kohno, H. *Phys. Rev. Lett.* **2004**, *92*, 086601.
(8) Hu, M. J.; Lu, Y.; Zhang, S.; Guo, S.-R.; Lin, B.; Zhang, M.; Yu, S.-H. *J. Am. Chem. Soc.* **2008**, *130*, 11606.
(9) Hu, M. J.; Lin, B.; Hu, S. H.; Nano Res. **2008**, *1*, 303, and references therein.
(10) Feng, S.; Zhao, J.; Du, G.; Song, C.; Song, J.; Zhu, Z. *J. Phys. Chem. C* **2008**, *112*, 15247.
(11) Thongmee, S.; Pang, H. L.; Yi, J. B.; Ding, J.; Lin, J. Y.; Van, L. H. *Acta Mater.* **2009**, *57*, 1482.
(12) Leng, Y.; Zhang, Y.; Liu, T.; Suzuki, M.; Li, X. *Nanotechnology* **2006**, *17*, 1797.
(13) Leng, Y.; Li, Y.; Li, X.; Takahashi, S. *J. Phys. Chem. C* **2007**, *111*, 6630.

Published on Web 01/26/2010

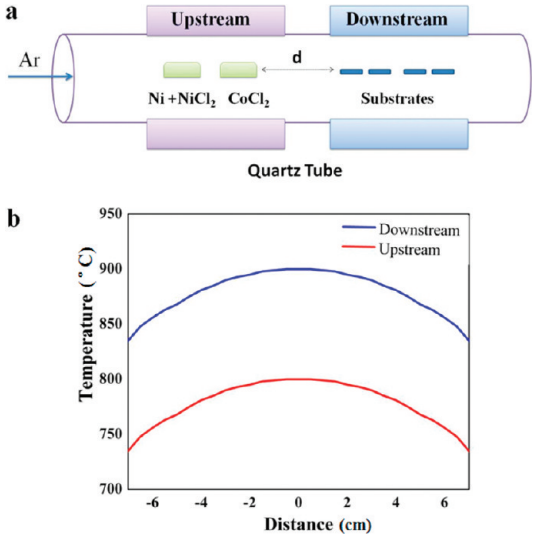

Figure 1. (a) Experimental setup. (b) Temperature profile during nanostructures growth.

Ni and Co, leading to production of various $Ni_{1-x}Co_x$ alloy NWs.

Experimental Section

Single-crystalline Ni_3Co NWs were synthesized using a hot wall dual-zone furnace employing 1 in. diameter quartz tube. Anhydrous $NiCl_2$ (Sigma-Aldrich, 99.99%) and $CoCl_2$ (Sigma-Aldrich, 99.99%) were used in stoichiometric amount as precursors. The upstream (US) zone and downstream (DS) zone were used for vaporization of precursor and the NW growth, respectively. The substrates were placed at ~12 cm from the precursor in the DS zone. The DS zone was initially heated to 900 °C, and then the U.S. zone was heated to 800 °C. The flow rate of carrier Ar gas was controlled in the range of 125−150 sccm, and the reaction time was 30 min. The samples were slowly cooled down to room temperature, which is essential to get single-crystalline NWs. At a higher flow rate of 150 sccm, random arrangement of NWs was observed, whereas vertical alignment was observed at a lower flow rate of 125 sccm. The density of NWs was strongly dependent on the DS temperature and substrate distance from the precursor. A lower DS temperature yielded a very low density of NWs, whereas a higher DS temperature resulted in the growth of two-dimensional nanostructures rather than NWs. Hence careful monitoring of reaction temperature and position of substrate is required in order to get a higher density of NWs on sapphire substrates.

Field emission scanning electron microscope (FESEM) images of Ni_3Co NWs were taken on a Phillips XL30S. Transmission electron microscope (TEM), high-resolution TEM (HRTEM) images, and selected area electron diffraction (SAED) patterns were taken on a JEOL JEM-2100F transmission electron microscope operated at 200 kV. After NWs were dispersed in ethanol, a drop of the solution was put on a holey carbon coated copper grid for the preparation of TEM analysis.

Results and Discussion

Single-crystalline nickel cobalt NWs have been synthesized in a hot wall dual-zone furnace using a chemical vapor transport method (Figure 1a) under various carrier gas flow rates and growth temperatures. A tilted field emission

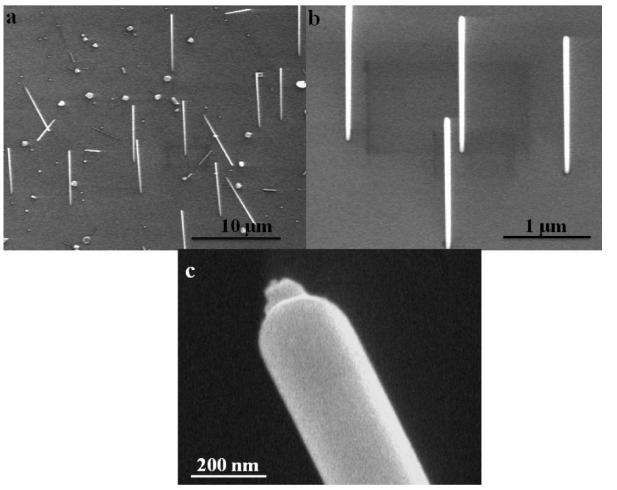

Figure 2. (a) Tilted view SEM image of vertically aligned Ni_3Co NWs on *c*-plane sapphire. (b) Magnified tilted view SEM image of Ni_3Co NW grown at 125 sccm. (c) Ni_3Co_2 alloy nanoparticle was found at the tip of a Ni_3Co NW.

SEM image of as synthesized NWs on a sapphire substrate is shown in Figure 2a, which demonstrates that the sample contains a large number of vertical NWs. A few NWs are inclined to the substrate. Figure 2b shows an enlarged SEM image of NWs revealing that the majority of NWs is vertically aligned to the substrate and has a length up to several micrometers. Figure 2c shows a magnified SEM image of a nanoparticle found at the tip of NWs. These nanoparticles are observed at the tip of all freestanding Ni_3Co NWs, suggesting that the nanoparticles may play a crucial role in the NW growth mechanism.

TEM image of Ni_3Co NW in Figure 3a shows that the NW has a smooth surface and a diameter of 100−120 nm with an about 10 nm thick oxide shell. The lattice resolved HRTEM image of Ni_3Co NW (Figure 3b) shows a lattice spacing of 0.25 nm between the adjacent planes in (110) growth direction. SAED pattern (Figure 3c) is well indexed to a face-centered-cubic (FCC) crystal structure of Ni (JCPDS card No. 01−1260, space group *Fm*3*m*). The single-crystalline nature of the NW is clear from the SAED pattern and the HRTEM images. SAED patterns collected at different zone axes were also indexed to an FCC crystal structure of Ni (Figure 4). Energy-dispersive X-ray spectrum (EDS) analysis performed on different selected areas of the NW shows that NW contains both nickel and cobalt with a mean atomic ratio of 77:23 (Figure 3d). The peak for Cu is from the TEM grid. Scanning TEM (STEM) image and its EDS mapping for a selected NW are shown in Figure 3e, suggesting that Ni and Co elements are distributed homogenously over the entire NW.

The growth mechanism of the Ni_3Co NWs was elucidated by TEM investigation of the NWs' tip. Both SEM and TEM images show nanoparticles at the tip of the NWs (Figures 2c and 5b). We propose a VSS mechanism to explain the growth of Ni_3Co NWs.[14] A magnified TEM

(14) Lensch-Falk, J. L.; Hemesath, E. R.; Perea, D. E.; Lauhon, L. J. *J. Mater. Chem.* **2009**, *19*, 849.

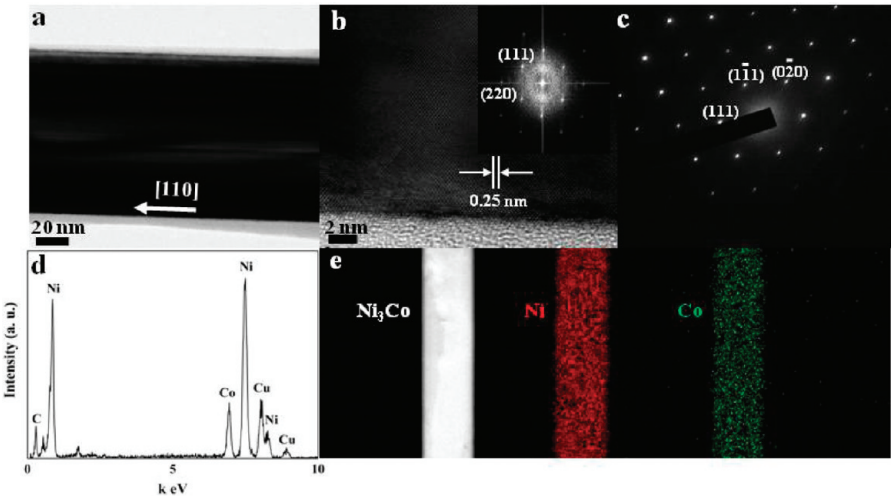

Figure 3. (a) TEM image of a Ni_3Co NW showing the oxide shell coating. (b) HRTEM image showing a distance of 0.25 nm between the adjacent planes corresponding to (110) planes. Inset shows FFT pattern that can be indexed to an FCC crystal structure of nickel. (c) SAED pattern down the [101] zone axis showing the single-crystalline nature of Ni_3Co NWs. (d) EDS spectrum of Ni_3Co NW showing the composition of Ni and Co in 3:1 ratio. (e) STEM image of Ni_3Co NW with corresponding EDS elemental mapping.

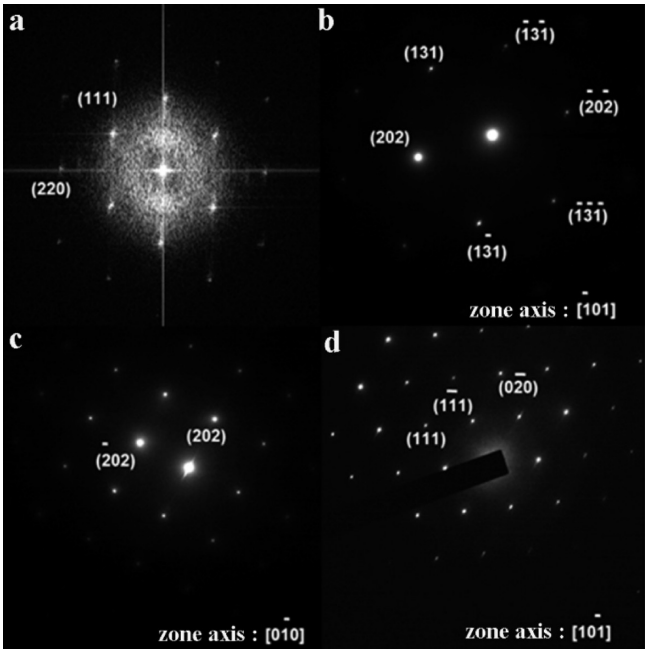

Figure 4. (a) FFT of HRTEM image of a Ni_3Co NW. (b-d) SAED patterns obtained from a representative Ni_3Co NW down the different zone axes. The SAED patterns of the NW at different zone axes show a regular spot pattern that can be indexed to an FCC Ni structure reflecting the single-crystalline nature of the NW.

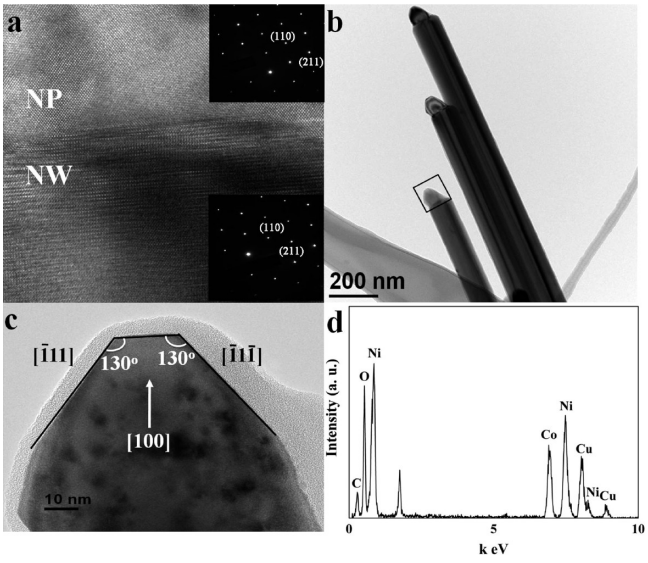

Figure 5. (a) Lattice-resolved TEM image of the interface of Ni_3Co NW and Ni_3Co_2 nanoparticle. Inset shows SAED patterns from Ni_3Co NW and Ni_3Co_2 nanoparticle, respectively. (b) Low-resolution TEM image of Ni_3Co NWs showing the presence of nanoparticle at the tip of individual NW. (c) The enlarged TEM image of faceted Ni_3Co_2 alloy nanoparticle from the rectangular region in panel b. (d) EDS spectrum from a single nanoparticle showing that Ni and Co are present in an approximately 3:2 atomic ratio.

image of the NW tip (Figure 5c) shows faceted morphology covered by an oxide shell. The angle between the facets of the nanoparticle is 130°, suggesting that the nanoparticles are bound by low energy (111) planes of an FCC crystal structure.[15] Figure 5a shows a high-resolution TEM image of nanoparticle−NW interface and the corresponding SAED patterns. Interestingly, the faceted particles at the tip of NWs were found to be single-crystalline. The SAED pattern shows a regular spot pattern that can be indexed to an FCC crystal structure of Ni. Note that the composition of single-crystalline particle is Ni_3Co_2.

Systematic analyses of the NWs morphology were conducted to provide insight into the growth mechanism. The incorporation of Ni catalyst or by the uncatalyzed decomposition on the surface of growing NW.[16] The uniform diameter of the Ni_3Co NW along the NW axis suggests that the decomposition of the metal chloride and Co during the growth process takes place either through the precursors occurs much faster at the Ni_3Co_2

(15) Zhou, H.; Kumar, D.; Kvit, A.; Tiwari, A.; Narayan, J. *J. Appl. Phys*. **2003**, *94*, 4841.

(16) Lensch-Falk, J. L.; Hemesath, E. R.; Lauhon, L. J. *Nano Lett*. **2008**, *8*, 2669.

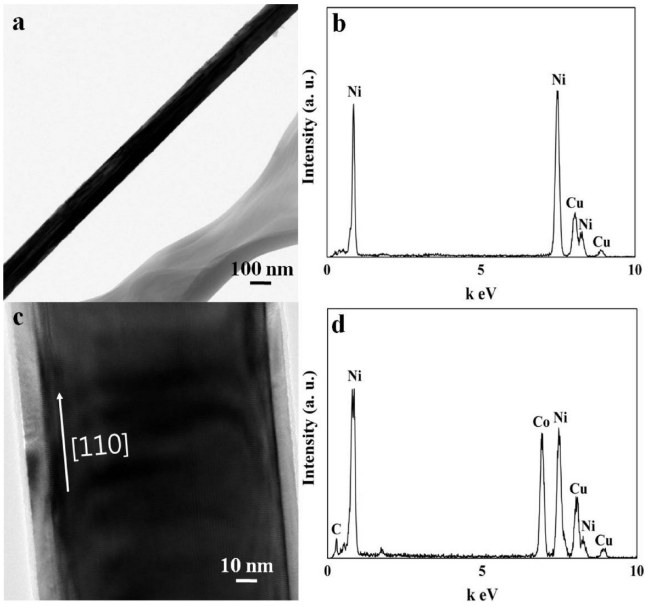

Figure 6. (a) TEM image of Ni NW ($x = 0$). (b) EDS pattern of Ni NW. (c) TEM image of a NiCo NW ($x = 0.5$) with growth direction parallel to the [110] direction. (d) EDS spectrum of an individual NiCo NW showing the peak intensity ratio of 1:1 for Ni and Co.

nanoparticles than at the surface of Ni_3Co NW (uncatalyzed decomposition) and the building blocks are supplied through the Ni_3Co_2 catalyst nanoparticle.[15−17] The NW growth interface acts as an effective sink for both Ni and Co adatoms, which subsequently get incorporated into a NW. Similar syntaxial synergistic growth of $Mn_{11}Ge_8$/Ge NW heterostructures has been reported.[15−17] Thus the Ni_3Co_2 nanoparticles at the tip of Ni_3Co NWs become an effective catalyst with the surface of the nanoparticle reducing the energy barrier for Ni and Co decomposition and acting as a nucleation site for incoming Ni and Co vapors.

The composition of NWs was tuned by changing the ratio of the amount of precursor metal chlorides in stoichiometry to get $Ni_{1-x}Co_x$ ($x = 0$, 0.25 and 0.5) alloy NWs. Growth times ranging from 15 to 60 min resulted in an average NW diameter of 100 nm and length exceeding several micrometers. TEM images and EDS spectrum of $Ni_{1-x}Co_x$ alloy NWs with $x = 0$ and 0.5 are shown in Figure 6. The equilibrium composition of $Ni_{1-x}Co_x$ alloy NWs is strongly dependent on the thermodynamic details of the thermal decomposition of metal chlorides and subsequent incorporation of adatoms into the catalyst. The modulation of Ni and Co composition in NWs is possible because of their comparable atomic radii, similar electronic structure, weakly segregating behavior, and thermodynamic stability of phases in entire composition range ($x = 0$ to 1).[18]

The magnetization of Ni_3Co NWs was investigated by zero-field-cooled (ZFC) and field-cooled (FC) magnetization at an applied field of 100 and 1000 Oe. Both $M-T$ curves of Ni_3Co NWs show typical ferromagnetic behavior with a Curie temperature above room temperature. The ZFC and FC curve of Ni_3Co NWs (Figure 7a) do not

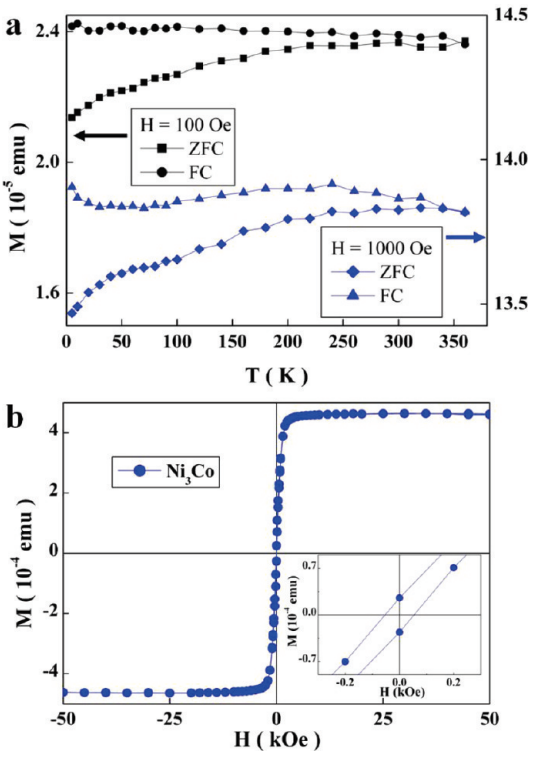

Figure 7. (a) M vs T measurement at 100 and 1000 Oe. (b) M vs H measurement of Ni_3Co NWs on c-plane sapphire at room temperature. Inset shows the magnified hysteresis loop between −0.3 and 0.3 kOe.

overlap at temperatures lower than room temperature, indicating that for the NWs a large magnetic anisotropy energy barrier distribution exists and a single domain size is not reached at these temperatures. Similar enhancement in the magnetic anisotropy has been reported in the case of two-dimensional nickel nanostructures.[12,13] Magnetic hysteresis of Ni_3Co NWs on c-plane sapphire was measured at room temperature under an applied field from −50 to 50 kOe. The hysteresis loop of NWs in Figure 7b reveals the ferromagnetic behavior at room temperature with the inset showing a magnified hysteresis loop between −0.3 and 0.3 kOe. Coercivity of 55 Oe was observed for Ni_3Co NWs. Note that these ferromagnetic Ni_3Co NWs contain an antiferromagnetic metal oxide shell (Figure 3a) that can exhibit additional magnetic anisotropy because of the exchange bias effect, which is observed at the ferromagnetic/antiferromagnetic interface.[19] Further experiments to understand the magnetic domains in nickel cobalt nanostructures and exchange bias are currently underway.

Conclusion

We have synthesized vertically aligned Ni_3Co NWs on sapphire substrates employing the chemical vapor transport method. A VSS mechanism was proposed for Ni_3Co NW growth, which was catalyzed by Ni_3Co_2 nanoparticles at the tip. The single-crystalline ferromagnetic Ni_3Co NWs as grown here with perpendicular

(17) Lensch-Falk, J. L.; Hemesath, E. R.; Lopez, F. J.; Lauhon, L. J. *J. Am. Chem. Soc.* **2007**, *129*, 10670.
(18) Novakovic, R.; Tanaka, T. *Physica B* **2006**, *371*, 223.
(19) Salgueiriño-Maceira, V.; Correa-Duarte, M. A.; Bañobre-López, M.; Grzelczak, M.; Farle, M.; Liz-Marzán, L. M.; Rivas, J. *Adv. Funct. Mater.* **2008**, *18*, 616.

magnetic anisotropy, thin diameter, and isotropic cross-section could be useful in future spintronics applications.

Acknowledgment. This research was supported by NRF through NRL (20090083138), SRC through "Center for Intelligent Nanobio Materials" (20090063004), and "Center for Nanostructured Materials Technology" (2009K000468) under "21st Century Frontier R&D Programs" of the MEST, Korea. SEM and TEM analysis were performed at the Korea Basic Science Institute in Daejeon.